

# Effect of Crystal and Domain Orientation on the Visible-Light Photochemical Reduction of Ag on BiFeO<sub>3</sub>

Andrew M. Schultz, Yiling Zhang, Paul A. Salvador, and Gregory S. Rohrer\*

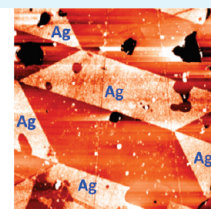
Department of Materials Science and Engineering, Carnegie Mellon University, Pittsburgh, Pennsylvania, United States

**ABSTRACT:** The reduction of silver from an aqueous solution on BiFeO<sub>3</sub> surfaces, activated by visible light, was investigated as a function of crystal and ferroelectric domain orientation. When excited by light with energy between 2.53 and 2.70 eV, BiFeO<sub>3</sub> photochemically reduces silver cations from solution in patterns corresponding to the underlying ferroelectric domain structure. Silver is preferentially reduced on domains with a positive polarization directed toward the surface. The amount of reduced silver depends on whether the component of the domain polarization normal to the surface is positive or negative, but is relatively insensitive to the crystal orientation. It is concluded that the ferroelectric polarization decreases electron drift to the surface in domains with a negative polarization, causing spatially selective photochemical behavior, and that the direction of the polarization is more important than the amplitude.

**KEYWORDS:** photochemistry, ferroelectric, BiFeO<sub>3</sub>, atomic force microscopy



BiFeO<sub>3</sub> (001) domain polarization map



BiFeO<sub>3</sub> (001) after visible light photochemical reduction of silver

## 1. INTRODUCTION

Spatially selective photochemical reactivity on the surfaces of ferroelectrics, initiated by the absorption of UV light, has been used to make nanoscale patterns of reduced metal.<sup>1–4</sup> The mechanism of the spatially selective reactivity is thought to be the spontaneous polarization in the ferroelectric domains, which bends the bands of electronic states so that photogenerated electrons and holes are transported in opposite directions.<sup>5–7</sup> As a result, electrons are transported to the surfaces of positive domains where reduction products form and holes are transported to the surfaces of negative domains where oxidation products form.<sup>8–15</sup>

Spatially selective reactivity induced by ferroelectric polarization may also be beneficial for water photolysis. The recombination of photogenerated charge carriers and the back reaction of intermediate species are major factors that limit the efficiency of water photolysis catalysts,<sup>16,17</sup> and it is possible that these processes will be mitigated by band bending in the domains. This concept has led to a number of studies involving water photolysis<sup>18–20</sup> and spatially selective reactivity on ferroelectric surfaces.<sup>1,8,10,11,14,15,21</sup> However, because the ferroelectrics used in the past have had relatively wide band gaps, they absorbed only a small fraction of the solar spectrum in the UV range. Therefore, even if losses due to recombination and back reaction are reduced, the overall efficiency suffers from the poor match of the energy levels with the solar spectrum.

The spatial selectivity of photochemical reactivity has been studied on BaTiO<sub>3</sub>,<sup>1,8,14,15</sup> LiNbO<sub>3</sub>,<sup>2</sup> and Pb(Zr<sub>0.3</sub>Ti<sub>0.7</sub>)O<sub>3</sub> (PZT),<sup>3,13</sup> all of which have band gaps larger than 3.0 eV. Here, we investigate the spatial selectivity of ferroelectric and semiconducting BiFeO<sub>3</sub>, which has a band gap of about 2.5 eV.<sup>22–24</sup> It has been reported BiFeO<sub>3</sub> can photochemically degrade organic compounds in visible light<sup>25,26</sup> and thin films of BiFeO<sub>3</sub> are

photoconductive in visible light.<sup>22</sup> Polycrystalline BiFeO<sub>3</sub> ceramics have a polarization of 6.1 μC cm<sup>-2</sup> along the ⟨111⟩ directions of the pseudo-cubic perovskite cell.<sup>27</sup> The purpose of this paper is to report on the spatially selective photochemical behavior of BiFeO<sub>3</sub> surfaces activated by visible light and the relative effects of grain orientation and domain orientation. The products of the reduction reaction correlated with the positions of ferroelectric domains with a positive component of the polarization perpendicular the BiFeO<sub>3</sub> surface. On the basis of this and other observations reported below, it is concluded that the ferroelectric polarization decreases electron drift to the surface in domains with a negative component of the polarization perpendicular the surface, causing spatially selective photochemical behavior that is more sensitive to domain orientation than crystal orientation.

## 2. EXPERIMENTAL SECTION

Bi<sub>2</sub>O<sub>3</sub> (Alfa Aesar, Ward Hill, MA, 99.99%) and Fe<sub>2</sub>O<sub>3</sub> (Alfa Aesar, 99.945%) powders were mixed in equal stoichiometric proportions. The mixture was ball-milled in ethanol with yttria-stabilized zirconia grinding media for 12 h. After evaporation of the ethanol at 85 °C, the dried powder was calcined at 650 °C for 6 h. The reacted powder was returned to the ball mill for an additional 12 h. After evaporation of ethanol, the powder was uniaxially compressed at 2.5 kPa into pellets using a few drops of a saturated solution of polyethylene glycol in ethanol as a binder. The samples were sintered in an alumina (99.6%) crucible with excess powder to minimize contamination from the crucible. The samples were heated to 600 °C for 12 h to burn off of the binder, sintered at 750 °C for 12 h, and annealed at 850 °C for 3 h to facilitate

**Received:** January 29, 2011

**Accepted:** April 25, 2011

**Published:** April 25, 2011

grain growth. Samples were lapped flat using a 9  $\mu\text{m}$  alumina slurry (Logitech, Glasgow, Scotland) and polished with a 0.02  $\mu\text{m}$  colloidal silica solution (Buehler, Lake Bluff, IL). Polished samples were thermally annealed at 500  $^{\circ}\text{C}$  for 3 h to repair polishing damage and create thermal grooves at the grain boundaries. Powder X-ray diffraction indicated that the majority phase was  $\text{BiFeO}_3$ . Small amounts of  $\text{Bi}_2\text{Fe}_4\text{O}_9$ ,  $\text{Bi}_{25}\text{FeO}_{40}$ , and  $\text{Fe}_2\text{O}_3$  were also detected in the diffraction pattern and will be referred to collectively in the remainder of the manuscript as minority phases.

The grain orientations within a 1 mm  $\times$  1 mm area were determined by electron backscatter diffraction (EBSD) mapping. Backscatter diffraction patterns were acquired using a Quanta 200 SEM (FEI, Hillsboro, OR). In a typical experiment, the sample was tilted at 70 $^{\circ}$  with respect to the beam, the working distance was 15 mm, the spot size was 5, and the accelerating voltage was 25 kV. Patterns were analyzed and indexed using TSL (Mahwah, NJ) orientation imaging microscopy data collection and analysis software. All patterns were indexed using a cubic reference frame, as the small rhombohedral distortion<sup>28</sup> of  $\text{BiFeO}_3$  is difficult to distinguish using EBSD. When analyzing the EBSD data, orientations with a confidence index less than 0.1 were removed and appear black in the resulting EBSD maps. Any collection of neighboring orientation points that were misoriented from each other by less than 5 $^{\circ}$  were assumed to belong to a single grain. The orientation of the grain was then determined by averaging the collection of individual orientation points associated with that grain.

Photochemical behavior was examined using the reduction of silver ions to neutral silver, depositing the insoluble silver on the surface.<sup>29,30</sup> This method is described previously for studies of titania and  $\text{BaTiO}_3$ .<sup>1,8,10,14,15,31,32</sup> Photochemical reactions were conducted by placing the sample in a small cylindrical container (diameter  $\sim$ 1 cm, height  $\sim$ 1 cm). The remaining volume was filled with 0.115 M solution of  $\text{AgNO}_3$  (Acros Organics, 99.85 %) in deionized water. A quartz coverslip was placed on top of the container and held in place by the surface tension of the solution. The assembly was illuminated for 30 min by a commercially available blue LED ( $\lambda_{\text{peak}} = 470$  nm, Philips Lumileds, San Jose, CA). The LED was powered by a DC supply, set to deliver a constant current of 100 mA and this corresponds to a power of 0.37 W. After reaction, the sample was rinsed with deionized water. The locations of the reaction products were then determined by AFM imaging. Only samples illuminated by the LED showed evidence of silver reduction; the surfaces of control samples left in the dark remained clean. X-ray diffraction of a sample illuminated for several hours (to increase the amount of reaction product) confirmed that metallic silver had been formed, consistent with previous findings on other oxides.<sup>1,31</sup>

Scanning probe characterization was performed using either an NT-MDT NTegra or Solver Next AFM/STM (NT-MDT, Moscow, Russia). Sample topography before and after photochemical reaction was determined using conventional contact or semicontact modes with similar results. Conventional methods were used for piezoresponse force microscopy (PFM) measurements.<sup>33</sup> In this case, a conductive TiN coated cantilever was used. For scanning tunneling spectroscopy measurements, a 80/20 PtIr tip was used.

### 3. RESULTS

An inverse pole figure map of the area of the sample used in this study is shown in Figure 1. Each pixel is colored by orientation according to the legend in Figure 1b. Typically, the undetermined orientations (black points) occur because there was a grain boundary, pore, or minority phase at that position. The regions of constant color correspond to grains of constant orientation. Twenty-four of these grains were selected for closer examination and their orientations are illustrated in Figure 1c.

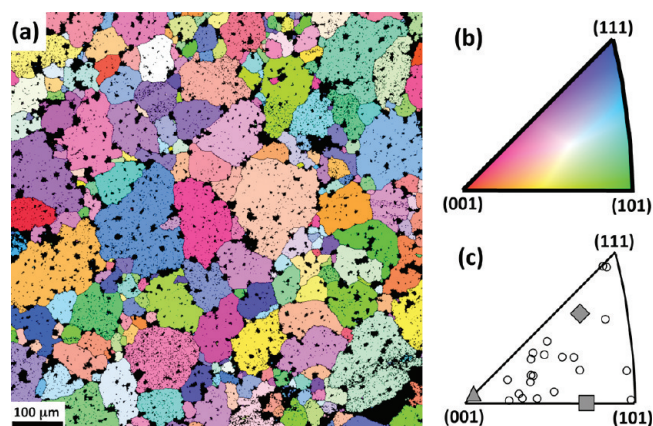


**Figure 1.** (a) Inverse pole figure map showing the grain orientations in the area of the polycrystalline  $\text{BiFeO}_3$  surface where the surface reactivity was determined. Each color corresponds to an orientation in (b). The orientations of the 24 grains that were studied in detail are illustrated in (c). The grains with orientations marked by the triangle, square, and diamond are discussed in more detail below.

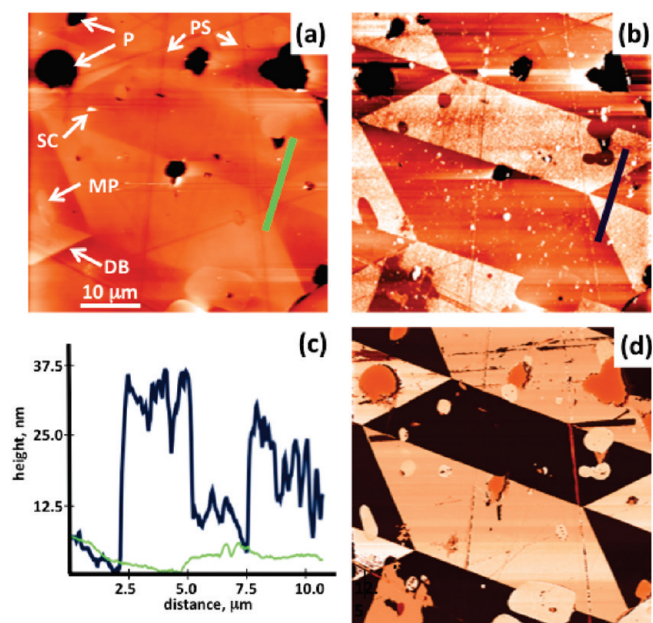


**Figure 2.** Topographic AFM images of  $\text{BiFeO}_3$  grain surface with a (001) orientation (a) before and (b) after the photochemical reduction of Ag. The topographic contrast in both images is 60 nm from bright to dark. (c) Height profile corresponding to the lines drawn in a and b demonstrating the height of silver deposits and the spatially selective nature of silver deposition. (d) Out-of-plane PFM phase image of the same area of the sample. Dark contrast in the image corresponds to regions with a  $-180^{\circ}$  phase shift (positive polarization) and bright regions correspond to a phase shift of  $0^{\circ}$  (negative polarization).

Each point in Figure 1c represents an orientation in the standard stereographic triangle of distinguishable crystal orientations.

AFM images of the grain with the orientation marked by the triangle in Figure 1c are shown in Figure 2. The surface orientation of this grain is, within the experimental uncertainty, (001). The same location is shown before and after the photochemical reduction of silver in images a and b in Figure 2, respectively. Topographic contrast in the AFM images arises

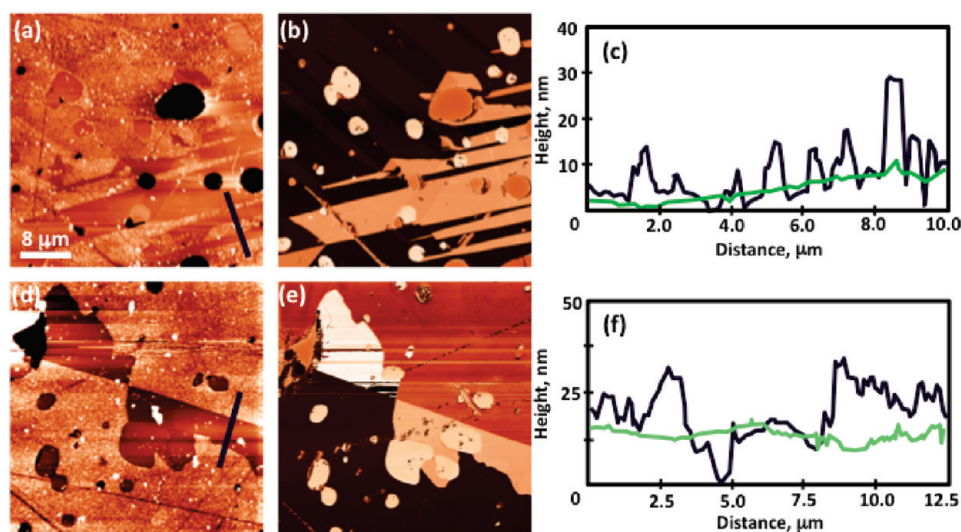


**Figure 3.** (a, d) Topographic images of BiFeO<sub>3</sub> grains after the photochemical reduction of silver. Light to dark contrast for both images is 60 nm. (b, e) Out-of-plane PFM phase images for the same areas. Dark contrast corresponds to a positive out of plane polarization. (c, f) Height profiles corresponding to the line drawn in a and d. The green lines show the topography before the reaction.

from pores (P), residual polishing scratches (PS), minority phases (MP), surface contamination (SC), and boundaries between ferroelectric domains (DB);<sup>34</sup> examples of each feature are labeled on the micrographs. In Figure 2b, the reduced silver corresponds to areas of bright contrast in the AFM images. The areas of silver deposition follow the areas of ferroelectric domains visible on the images of the clean surface and the heights of the silver deposits vary between 20 and 130 nm. Height profiles are depicted in Figure 2c for the lines drawn in the AFM images shown in images a and b in Figure 2 before and after the reaction. This direct comparison of the same area of the sample shows a clear distinction in heights for domains before and after the reduction of silver.

After the silver was removed from the sample surface, the sample was returned to the microscope and the same area was examined using piezoresponse force microscopy (PFM). The silver was removed by wiping the surface with a cotton swab and rinsing with deionized water. AFM scans after cleaning show that all silver was removed from the sample. Figure 2d shows a PFM phase image for the same area of the sample surface depicted in images a and b in Figure 2. The direction of the polarization vector determines the phase lag between the AC bias of the tip and the deflection. Throughout this paper, domains with a positive out-of-plane polarization will be referred to as “positive” domains and domains with a negative out-of-plane polarization will be referred to as “negative” domains. In the PFM images, the phase lag is 180° for positive domains and 0° for negative domains.<sup>35–38</sup> Areas of silver deposition correspond to domains that appear dark in the PFM image. These areas correspond to a phase lag of 180°, consistent with positive domains. Bright areas in the PFM image, consistent with negative domains, correspond to areas without significant silver reduction.

The domain polarization is along  $\langle 111 \rangle$  type directions and the orientations of the boundaries between domains are  $\{110\}$  and  $\{100\}$  type planes for 71° and 109° domain boundaries, respectively.<sup>34</sup> For 180° boundaries, where the polarization vectors are anti-parallel, the plane can take any orientation in the zone of  $[111]$ . Therefore, in the general case, we can expect to see both straight and wavy boundaries. When the 71 and 109°

domain boundaries intersect the (001) surface, they create traces that intersect at 45 and 90°. Note that all of the straight lines that appear to be domain boundaries in Figure 2 are consistent with these expected angles. Grains of other orientations consistently showed either straight lines traversing the entire grain, or combinations of straight and curved boundaries as illustrate in Figure 3.

Figure 3 shows AFM topography, PFM phase, and height profile comparisons for two additional grains of the 24 orientations in Figure 1c. The orientation of the grain in Figure 3a is indicated by the diamond in Figure 1c and the orientation of the grain in Figure 3d is indicated by the square. These results, and those shown in Figure 2, are representative of all of the orientations. Silver was reduced on the surface in patterns corresponding to the underlying domain structure. Positive domains promoted silver reduction and negative domains had little to no solid product on the surface after reaction. The amounts of silver reduced on the surfaces shown in Figure 3 are similar to the amounts in Figure 2 and are characteristic of all of the grain orientations in Figure 1c. In other words, no systematic variation in reactivity could be detected as a function of orientation.

To probe the electronic properties of the sample, current–voltage curves were acquired in the scanning tunneling spectroscopy mode. Because this was done in air, we assume that the tip is actually in weak contact with the sample. Current–voltage curves were acquired at periodic positions on the surface and all appeared similar. A typical curve is shown in Figure 4, where rectifying behavior is observed; current flows from the sample to the tip at all positive biases but no current flows from the tip to the sample until the tip is at least one volt more negative than the sample. This behavior is characteristic of a p-type semiconductor where the Fermi level is near the lower edge of the band gap. When the tip is positive with respect to the sample, electrons flow from occupied states in the valence band to the tip. When the tip is made more negative than the sample, the Fermi level of the tip moves through the band gap of the sample until it reaches empty states near the conduction band edge, and electrons can then flow from the tip to the sample. A simple two-point resistivity measurement showed that the

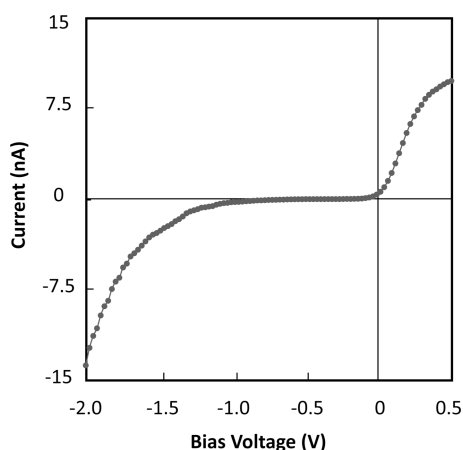


**Figure 4.** Current versus tip bias measured in a scanning tunneling spectroscopy experiment on the surface of BiFeO<sub>3</sub>.

sample was only weakly conductive and had a resistivity of approximately  $1 \times 10^7$  ohm-cm.

#### 4. DISCUSSION

The results presented here indicate that the photochemical reduction of silver, initiated by visible light, is spatially selective on the BiFeO<sub>3</sub> surface. This is similar to what has been observed previously on BaTiO<sub>3</sub>, SrTiO<sub>3</sub>, and PZT when illuminated under UV light.<sup>1,12,14,31,32,39</sup> Here we propose a model for the surface electronic band structure of BiFeO<sub>3</sub>, and how it is affected by ferroelectric polarization, to explain the observed reactivity. The proposed energy level structure, shown in Figure 5, is based upon a number of assumptions. First, the electron affinity of the BiFeO<sub>3</sub> (4.6 eV) was approximated using the method described by Morrison.<sup>40</sup> The band gap of BiFeO<sub>3</sub> has been reported over a wide range (2.2–2.7 eV) in different sources;<sup>22–24</sup> in the construction of Figure 5, we assumed a band gap of 2.5 eV. Most reports in the literature indicate that BiFeO<sub>3</sub> is p-type<sup>41,42</sup> and this is consistent with the current–voltage response shown in Figure 4.

Figures 5a and 5b compare the band positions in bulk BiFeO<sub>3</sub> with those near the surface when in contact with solution, with no out-of-plane polarization. Interface states cause downward band bending at the surface of a p-type semiconductor in contact with water.<sup>40</sup> In this case, electron-hole pairs generated within the depletion region are driven apart by the electric field. Electrons are driven towards the surface and holes are driven away from the surface. When electrons reach the surface, they can reduce adsorbed species. Panels c and d in Figure 5 show the effect of ferroelectric polarization on the band bending near the surface. The polarization vector in positive domains, depicted in Figure 5c, causes an increased accumulation of negative charge just below the surface. Band edge energies are driven further downward and the driving force for electrons to reach the surface and participate in photochemical reduction is increased. The opposite is true for a negative domain, which is depicted in Figure 5d. The negative out-of-plane component of polarization causes an increase in positive charge just below the surface and this reduces the downward band bending. If the magnitude of the polarization vector is large enough, the bands bend upwards. We take the experimental observation that silver does not reduce on the surfaces of negative domains as evidence that the bands are

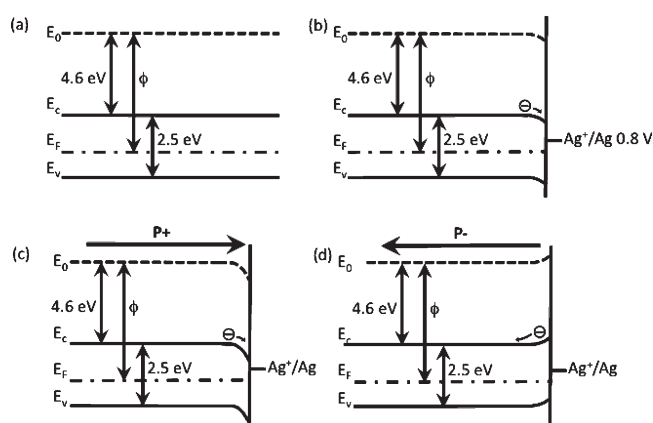


**Figure 5.** Schematic band diagrams for BiFeO<sub>3</sub>. In the figure,  $\phi$  is the work function,  $E_0$ ,  $E_c$ ,  $E_F$ , and  $E_v$  are the energy levels of a free electron, the conduction band edge, the Fermi level, and the valence band edge, respectively. (a) Bands in bulk BiFeO<sub>3</sub>. (b) Bands of BiFeO<sub>3</sub> in contact with solution, with the standard redox potential for Ag<sup>+</sup>/Ag labeled vs the normal hydrogen electrode. (c) Bands in contact with solution and a positive out-of-plane polarization. (d) Bands in contact with solution and a negative out-of-plane polarization.

bent upward and depict them as such in Figure 5d, creating a barrier for electrons. In other words, photogenerated electrons within the band bending region are driven away from the surface and this shuts off the silver reduction reaction in these domains. Because electrons and holes are driven to different areas of the surface, the chances of charge carrier recombination are reduced. Additionally, intermediate species produced during the reaction are located in physically separate areas of the surface, reducing back reaction. Because of this, the fields generated by the ferroelectric polarization might improve the efficiency of photochemical reactions. Finally, we note that throughout this discussion, we have ignored the effect of adsorption from the solution. In this case, we would expect aqueous Ag<sup>+</sup> cations to enrich or adsorb at the surfaces of negative domains and be repelled from positive domains. Because reduced silver is found only on the positive domains, the observed spatially selective reactivity is not consistent with adsorption processes.

There are two possible mechanisms for the orientation dependence of the reactivity of a ferroelectric material. The first is that photochemical reactions on metal oxides are anisotropic.<sup>31,32,39,43,44</sup> While the origins of this anisotropy have not been clearly established, they are presumably connected to the orientation dependence of surface structure, composition, and the exact positions of band edges on the surface.<sup>39,45</sup> This phenomenon is potentially important in the design of a photolysis catalyst.<sup>46</sup>

The second mechanism by which crystal orientation might affect reactivity relates to the crystallographic restrictions on domain polarization. For a given ferroelectric material, the direction of ferroelectric polarization is limited to a distinct set of crystal directions. In the case of BiFeO<sub>3</sub>, the polarization occurs along the  $\langle 111 \rangle$  family of directions.<sup>27</sup> The out-of-plane component of the polarization vector is thought to play the most significant role in affecting photochemical activity. Varying the grain orientation changes the possible values of the out-of-plane component of each of the possible polarization directions. For example, a (111)-oriented crystal can have two antiparallel polarization vectors pointing perpendicular to the surface. The

remaining six directions point  $29^\circ$  above or below the surface plane, greatly reducing the out of plane component of polarization. In the case of a (001)-oriented grain, all of the polarization vectors point  $54^\circ$  above or below the surface, resulting in an equal out-of-plane magnitude of polarization for all directions. Dunn and co-workers<sup>13</sup> reported on differences in the photochemical reduction of Ag on (001) and (111) oriented PZT, finding that that positive domains in films of both orientations have a similar reactivity, but that negative domains completely stop the reactivity only on the (111) orientation where the polarization is perpendicular to the surface. Burbure and co-workers<sup>10</sup> reported on the relative reactivity of (001), (011), and (111) BaTiO<sub>3</sub> (which is polarized along [100]), and found comparable activity for reduction on all three surfaces.

In the current study, spatially selective reactivity was observed for all grain orientations. Contrary to the observations on PZT thin films, even grains with the (001) orientation strongly suppress the reduction of silver in the negative domains (see Figure 2). This difference cannot be explained by differences in the polarization: PZT is reported to have a larger remnant polarization than BiFeO<sub>3</sub> and that would favor increased spatial selectivity in PZT, counter to what is observed.<sup>47</sup> It is possible that differences in the microstructure might account for differences in the reactivity. The BiFeO<sub>3</sub> crystals studied here were many tens of micrometers in extent, while the PZT was a 70 nm thick film with grains of similar sizes.<sup>13</sup> Because there are geometric constraints on the development of space charges in nano-sized grains, it is possible that the band bending regions are larger in the microcrystalline BiFeO<sub>3</sub> samples studied here.<sup>48</sup>

While the differences between BiFeO<sub>3</sub> and PZT cannot be resolved from the present observations, the results presented here demonstrate that the ferroelectric domain structure is more important than grain orientation in determining surface reactivity. In grains where ferroelectric domains are present, reactivity was observed to be selective and the heights of reduced silver on the reactive domains did not systematically depend on grain orientation. This lack of a strong anisotropy in reactivity indicates that the relative orientation of the polarization vector is sufficient in BiFeO<sub>3</sub> to control the spatial selectivity, consistent with previously published results for BaTiO<sub>3</sub>.<sup>49</sup> If the relative magnitude of the polarization normal to the surface determined local reactivity, then (111) oriented BiFeO<sub>3</sub> grains should have the greatest reactivity in domains with a positive polarization points toward the outer surface. However, the reactive domains on grains oriented near (111) were not noticeably more reactive than reactive domains on grains with different orientations. The same is true for the unreactive, negative domains, where the bands bend upward. A possible explanation for this behavior is found by comparing the depletion layer width and the penetration depth of the illumination. If the photon penetration depth is smaller than the space charge region that results from the ferroelectric polarization, increasing the width of the space charge layer causes no increase in reactivity. All photogenerated charge carriers are already created within the space charge region and driven to or from the surface. Yang et al.<sup>50</sup> estimate a depletion layer width of 300 nm for BiFeO<sub>3</sub>. The penetration depth for 460 nm light in BiFeO<sub>3</sub> is approximately 36 nm, using the extinction coefficient data from Kumar et al.<sup>51</sup> In this case, the space charge region is much larger than the penetration depth, and any increase in the width of the space charge region will not increase the photochemical reactivity of the material. As a result, in any domains where the bands are bend downward, silver is

reduced, and in any domains where they are bent upward, no silver is reduced.

It has recently been shown that thin titania films supported by BiFeO<sub>3</sub> are also active for silver reduction using the same light source.<sup>52</sup> This indicates that it should be possible to create a heterostructured core-shell photocatalyst of BiFeO<sub>3</sub> particles coated by a thin layer of titania that will combine the favorable band edge positions and stability of the titania surface with the light absorbing and charge separating characteristics of the BiFeO<sub>3</sub> core. The present results suggest that in such a composite material, the shape of the BiFeO<sub>3</sub> crystals will not be important, but the size will. To effectively absorb light, the cores will have to be at least twice the absorption depth and to effectively separate charge, they should be large enough to sustain a ferroelectric polarization that promotes band bending, and this is twice the width of the space charge region. Because these two lengths will not generally be the same, the reactivity may be size dependent.

## 5. CONCLUSION

BiFeO<sub>3</sub> surfaces exhibit spatially selective visible-light photochemical activity. Silver ions in solution were photochemically reduced by the BiFeO<sub>3</sub>, depositing solid silver on the surface in patterns corresponding to positive ferroelectric domains. Upward band bending in the negative domains prevents electrons from reaching the surface and these locations do not reduce silver. Electric fields arising from ferroelectric domains at the surface overwhelm anisotropy in the photochemical activity that might arise from grain orientation alone.

## AUTHOR INFORMATION

### Corresponding Author

\*E-mail: rohrer@cmu.edu.

## ACKNOWLEDGMENT

The work was supported by National Science Foundation Grant DMR 0804770.

## REFERENCES

- (1) Giocondi, J. L.; Rohrer, G. S. *J. Phys. Chem. B* **2001**, *105*, 8275–8277.
- (2) Hanson, J. N.; Rodriguez, B. J.; Nemanich, R. J.; Gruverman, A. *Nanotechnology* **2006**, *17*, 4946–4949.
- (3) Kalinin, S. V.; Bonnell, D. A.; Alvarez, T.; Lei, X.; Hu, Z.; Ferris, J. H.; Zhang, Q.; Dunn, S. *Nano Lett.* **2002**, *2*, 589–593.
- (4) Tiwari, D.; Dunn, S. *J. Mater. Sci.* **2009**, *44*, 5063–5079.
- (5) Brody, P. S. *Solid State Commun.* **1973**, *12*, 673–676.
- (6) Brody, P. S. *J. Solid State Chem.* **1975**, *12*, 193–200.
- (7) Fridkin, V. M. *Ferroelectrics* **1984**, *53*, 169–187.
- (8) Bhardwaj, A.; Burbure, N. V.; Gamalski, A.; Rohrer, G. S. *Chem. Mater.* **2010**, *22*, 3527–3534.
- (9) Burbure, N. V.; Salvador, P. A.; Rohrer, G. S. *J. Am. Ceram. Soc.* **2006**, *89*, 2943–2945.
- (10) Burbure, N. V.; Salvador, P. A.; Rohrer, G. S. *Chem. Mater.* **2010**, *22*, 5831–5837.
- (11) Burbure, N. V.; Salvador, P. A.; Rohrer, G. S. *Chem. Mater.* **2010**, *22*, 5823–5830.
- (12) Dunn, S.; Jones, P. M.; Gallardo, D. E. *J. Am. Chem. Soc.* **2007**, *129*, 8724–8728.
- (13) Dunn, S.; Tiwari, D.; Jones, P. M.; Gallardo, D. E. *J. Mater. Chem.* **2007**, *17*, 4460–4463.

- (14) Giocondi, J. L.; Rohrer, G. S. *Chem. Mater.* **2001**, *13*, 241–242.
- (15) Giocondi, J. L.; Rohrer, G. S. *Top. Catal.* **2008**, *49*, 18–23.
- (16) Domen, K. In *Surface Photochemistry*; J. Wiley & Sons: Chichester, U.K., 1996; p 1.
- (17) Kudo, A.; Miseki, Y. *Chem. Soc. Rev.* **2009**, *38*, 253–278.
- (18) Inoue, Y. *Energy Environ. Sci.* **2009**, *2*, 364–386.
- (19) Inoue, Y.; Hayashi, O.; Sato, K. *J. Chem. Soc., Faraday Trans.* **1990**, *86*, 2277–2282.
- (20) Inoue, Y.; Sato, K.; Miyama, H. *J. Phys. Chem.* **1986**, *90*, 2809–2810.
- (21) Bhardwaj, A.; Burbure, N. V.; Rohrer, G. S. *J. Am. Ceram. Soc.* **2010**, *93*, 4129–4134.
- (22) Basu, S. R.; Martin, L. W.; Chu, Y. H.; Gajek, M.; Ramesh, R.; Rai, R. C.; Xu, X.; Musfeldt, J. L. *Appl. Phys. Lett.* **2008**, *92*, 091905.
- (23) Choi, T.; Lee, S.; Choi, Y. J.; Kiryukhin, V.; Cheong, S. W. *Science* **2009**, *324*, 63–66.
- (24) Gao, F.; Yuan, Y.; Wang, K. F.; Chen, X. Y.; Chen, F.; Liu, J. M. *Appl. Phys. Lett.* **2006**, *89*, 102506.
- (25) Cho, C. M.; Noh, J. H.; Cho, I. S.; An, J. S.; Hong, K. S.; Kim, J. Y. *J. Am. Ceram. Soc.* **2008**, *91*, 3753–3755.
- (26) Gao, F.; Chen, X. Y.; Yin, K. B.; Dong, S.; Ren, Z. F.; Yuan, F.; Yu, T.; Zou, Z.; Liu, J. M. *Adv. Mater.* **2007**, *19*, 2889–2892.
- (27) Teague, J. R.; Gerson, R.; James, W. J. *Solid State Commun.* **1970**, *8*, 1073–1074.
- (28) Kubel, F.; Schmid, H. *Acta Crystallogr., Sect. B* **1990**, *46*, 698–702.
- (29) Clark, W. C.; Vondjidi, A. G. *J. Catal.* **1965**, *4*, 691–696.
- (30) Herrmann, J. M.; Disdier, J.; Pichat, P. *J. Catal.* **1988**, *113*, 72–81.
- (31) Lowekamp, J.; Rohrer, G.; Hotsenpiller, P.; Bolt, J.; Farneth, W. *J. Phys. Chem. B* **1998**, *102*, 7323–7327.
- (32) Hotsenpiller, P.; Bolt, J.; Farneth, W.; Lowekamp, J.; Rohrer, G. *J. Phys. Chem. B* **1998**, *102*, 3216–3226.
- (33) Christman, J. A.; Woolcott, R. R.; Kingon, A. I.; Nemanich, R. J. *Appl. Phys. Lett.* **1998**, *73*, 3851–3853.
- (34) Catalan, G.; Scott, J. F. *Adv. Mater.* **2009**, *21*, 2463–2485.
- (35) Kalinin, S. V.; Bonnell, D. A. *Phys. Rev. B* **2001**, *63*, 125411.
- (36) Kalinin, S. V.; Bonnell, D. A. *Phys. Rev. B* **2002**, *65*, 125408.
- (37) Kalinin, S. V.; Eliseev, E. A.; Morozovska, A. N. *Appl. Phys. Lett.* **2006**, *88*, 232904.
- (38) Kalinin, S. V.; Karapetian, E.; Kachanov, M. *Phys. Rev. B* **2004**, *70*, 184101.
- (39) Giocondi, J. L.; Rohrer, G. S. *J. Am. Ceram. Soc.* **2003**, *86*, 1182–1189.
- (40) Morrison, S. R. *Electrochemistry at Semiconductor and Oxidized Metal Electrodes*; Plenum Press: New York, 1980; p 137.
- (41) Vengalis, B.; Devenson, J.; Oginskis, A. K.; Butkute, R.; Maneikis, A.; Steikonienė, A.; Dapkus, L.; Banys, J.; Kinka, M. *Acta Phys. Pol., A* **2008**, *113*, 1095–1098.
- (42) Yang, H.; Luo, H. M.; Wang, H.; Usov, I. O.; Suvorova, N. A.; Jain, M.; Feldmann, D. M.; Dowden, P. C.; DePaula, R. F.; Jia, Q. X. *Appl. Phys. Lett.* **2008**, *92*, 102113.
- (43) Ohno, T.; Sarukawa, K.; Matsumura, M. *New J. Chem.* **2002**, *26*, 1167–1170.
- (44) Taguchi, T.; Saito, Y.; Sarukawa, K.; Ohno, T.; Matsumura, M. *New J. Chem.* **2003**, *27*, 1304–1306.
- (45) Giocondi, J. L.; Salvador, P. A.; Rohrer, G. S. *Top. Catal.* **2007**, *44*, 529–533.
- (46) Sosnowchik, B. D.; Chiamori, H. C.; Ding, Y.; Ha, J. Y.; Wang, Z. L.; Lin, L. W. *Nanotechnology* **2010**, *21*, 485601.
- (47) Kobayashi, T.; Ichiki, M.; Tsaui, J.; Maeda, R. *Thin Solid Films* **2005**, *489*, 74–78.
- (48) Albery, W. J.; Bartlett, P. N. *J. Electrochem. Soc.* **1984**, *131*, 315–325.
- (49) Burbure, N. V.; Salvador, P. A.; Rohrer, G. S. *J. Am. Ceram. Soc.* **2010**, *93*, 2530–2533.
- (50) Yang, S. Y.; Martin, L. W.; Byrnes, S. J.; Conry, T. E.; Basu, S. R.; Paran, D.; Reichertz, L.; Ihlefeld, J.; Adamo, C.; Melville, A.; Chu, Y. H.; Yang, C. H.; Musfeldt, J. L.; Schlom, D. G.; Ager, J. W.; Ramesh, R. *Appl. Phys. Lett.* **2009**, *95*, 062909.
- (51) Kumar, A.; Rai, R. C.; Podraza, N. J.; Denev, S.; Ramirez, M.; Chu, Y. H.; Martin, L. W.; Ihlefeld, J.; Heeg, T.; Schubert, J.; Schlom, D. G.; Orenstein, J.; Ramesh, R.; Collins, R. W.; Musfeldt, J. L.; Gopalan, V. *Appl. Phys. Lett.* **2008**, *92*, 121915.
- (52) Zhang, Y.; Schultz, A. M.; Salvador, P. A.; Rohrer, G. S. *J. Mater. Chem.* **2011**, *21*, 4168–4174.